The effect of the induced magnetic field on the electron density vertical profile of the Mars' ionosphere: A Mars Express MARSIS radar data analysis and interpretation, a case study

M. Ramírez-Nicolás, B. Sánchez-Cano, O. Witasse, P. -L. Blelly, L. Vázquez, M. Lester

Planetary and Space Science 126 (2016) 49–62

Contents lists available at ScienceDirect

Planetary and Space Science

journal homepage: www.elsevier.com/locate/pss

The effect of the induced magnetic field on the electron density vertical profile of the Mars' ionosphere: A Mars Express MARSIS radar data analysis and interpretation, a case study

M. Ramírez-Nicolás [a,b], B. Sánchez-Cano [c], O. Witasse [d,*], P.-L. Blelly [e], L. Vázquez [f,b], M. Lester [c]

[a] Universidad Complutense de Madrid, Facultad de Ciencias Fisicas, Avda. Complutense s/n, 28040 Madrid, Spain
[b] Instituto de Matemática Interdisciplinar (IMI), 28040 Madrid, Spain
[c] Radio and Space Plasma Physics Group, Department of Physics and Astronomy, University of Leicester, University Road, Leicester LE1 7RH, United Kingdom
[d] European Space Agency, ESTEC, Scientific Support Office, Keplerlaan 1, 2200 AG Noordwijk, The Netherlands
[e] Institut de Recherche en Astrophysique et Planetologie 9, Avenue du Colonel Roche, 31028 Toulouse Cedex 4, France
[f] Universidad Complutense de Madrid, Facultad de Informática, 28040 Madrid, Spain

ARTICLE INFO

Article history:
Received 4 April 2015
Received in revised form
26 February 2016
Accepted 22 March 2016
Available online 6 April 2016

Keywords:
Mars
Ionosphere
Induced magnetic field
Mars Express

ABSTRACT

We report the indirect detection of an induced magnetic field in the ionosphere of Mars and its effects on the electron density behaviour. The observations were made by the Mars Advanced Radar for Subsurface and Ionospheric Sounding (MARSIS) aboard Mars Express, in its Active Ionospheric Sounding mode. During several orbits on June 2006, the ionosphere showed an unusual behaviour, characterised by a compression of the plasma above the main ionospheric peak as observed by the topside total electron content, the plasma scale height, and the local plasma in the Mars Express surroundings. The compression was most likely due to an induced magnetic field originating from the solar wind and measured by the MARSIS antennas, which was able to penetrate into the ionosphere. In particular, for several profiles, the density distribution can be clearly defined by two different plasma scale heights, which indicates a transition region between both of them. From the balance of magnetic and thermal plasma pressures and from a comparison with a numerical model of the Martian ionosphere, the hypothesis of a penetrating induced magnetic field down to a transition altitude around 150 km is confirmed. This compressed ionosphere has also been compared with data from other orbits in the same location and at the same time period, i.e. 18.5 days of difference between first and last orbits, where there is no measured induced magnetic field, and the orbits show a clearly different behaviour.

1. Introduction

Mars Express (MEX) is the first mission of the European Space Agency (ESA) to any planet. The spacecraft was launched on 2nd June 2003 from the Baikonur Cosmodrome in Kazakhstan aboard a Russian Soyuz rocket (Chicarro et al., 2004). One of the objectives of the mission is to characterize in detail how the upper atmosphere of Mars, and in particular its ionosphere, is affected by external drivers such as solar wind events. Mars does not possess a global-scale internal magnetic field (e.g. Acuña et al., 1998; Connerney et al., 1999), and as a result, a direct and strong interaction between the upper atmosphere and the solar wind takes place.

The direct impact of the solar wind on the Mars environment produces a bow shock (BS) (Edberg et al., 2008 and references therein). After this shock, a magnetic pileup boundary (MPB) of the interplanetary magnetic field (IMF) in front of Mars is formed, essentially due to a pressure balance between the solar wind thermal pressure in the magnetosheath and the induced magnetic pressure (Dubinin et al., 2008b; Edberg et al., 2009). If one looks into this boundary from the plasma point of view, it can be also called the induced magnetosphere boundary (IMB), since it corresponds with the height where the plasma solar wind (energy of ions and electrons) strongly decreases (Lundin et al., 2004). Finally, the last and deeper boundary detected by Mars Express and Mars Global Surveyor (MGS) is the photo-electron boundary (PEB) (Frahm et al., 2006). This boundary marks the end of where the IMF can penetrate into the ionosphere. The ionopause is the region in which the solar wind plasma stops and the ionospheric plasma begins (Cravens, 1997). In other words, it is the region where a

* Corresponding author.
E-mail address: owitasse@cosmos.esa.int (O. Witasse).

http://dx.doi.org/10.1016/j.pss.2016.03.017

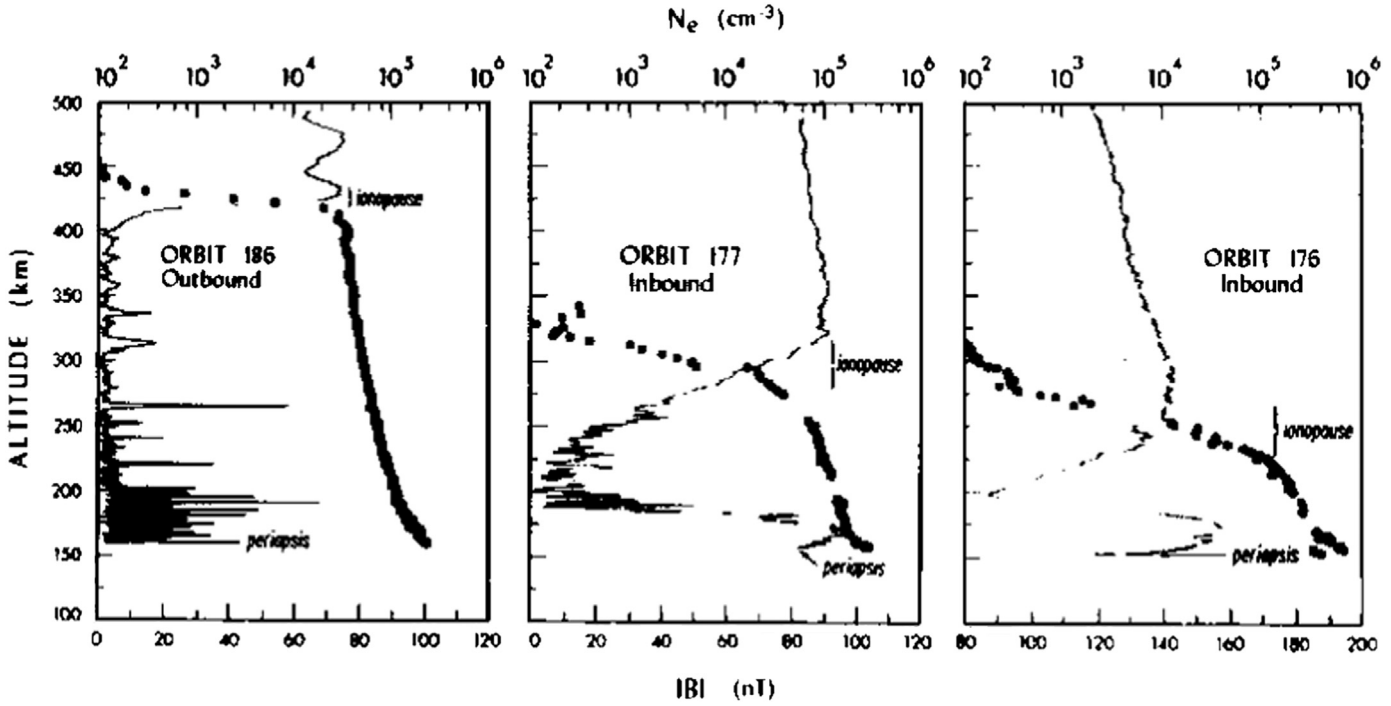

Fig. 1. Measured magnetic field strength (solid line, bottom scale) and electron densities profiles (solid dots, upper scale) of the ionosphere of Venus by Pioneer Venus Orbiter spacecraft for three different orbits (from Fig. 12 of Russell, 1992).

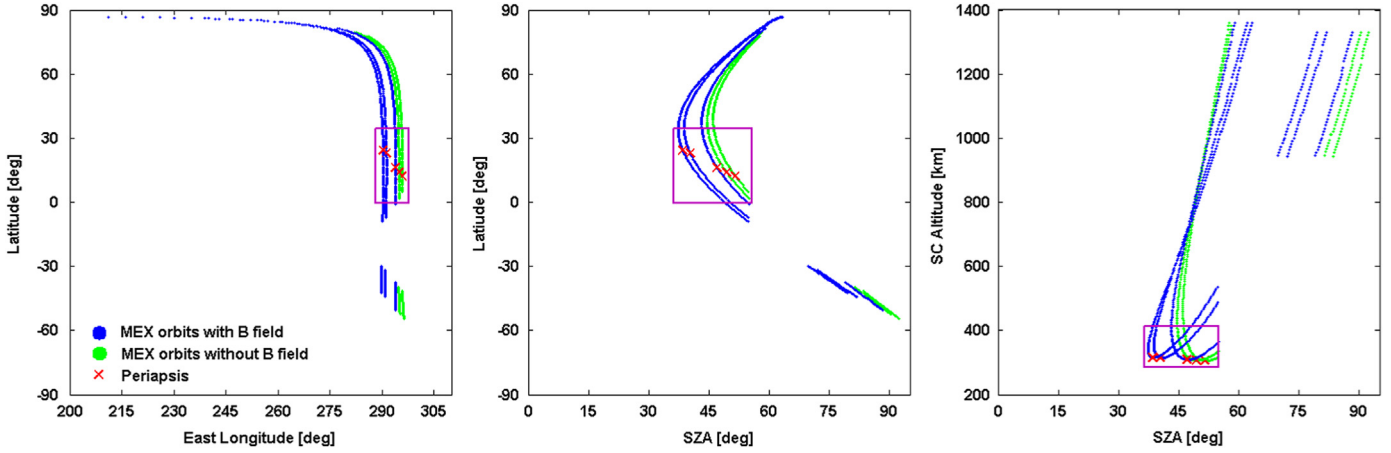

Fig. 2. Mars Express trajectory when MARSIS-AIS was in operation during the 5 orbits of this study. Left panel shows the latitude – longitude configuration. Medium panel shows the Latitude – solar zenith angle distribution and right panel, the spacecraft evolution with solar zenith angle. Orbits with magnetic field are in blue in the three panels, and orbits without magnetic field are in green. Pericenter is marked with a cross in all the cases. Data used in this study is indicated with a purple rectangle. (For interpretation of the references to colour in this figure legend, the reader is referred to the web version of this article.)

pressure balance between the ionosphere (thermal electron population) and the solar wind is found.

When the ionospheric thermal pressure is not large enough to withstand the solar wind dynamic pressure, the ionosphere can become magnetized, similarly to the Venus case (e.g. Shinagawa and Cravens, 1989, 1992; Zhang and Luhmann, 1992; Russell, 1992; Krymskii, 1992; Krymskii et al., 1995; Shinagawa, 1996; Shinagawa, 2004). The effect of this magnetisation on the electron density vertical profile in the case of Venus is best illustrated in Fig. 1 of this paper (Fig. 12 of Russell, 1992; Russell et al., 1983). The stronger the magnetic field is at the top of the ionosphere, the deeper it penetrates. The result is a clear compression of the ionosphere, characterised by a lower scale height (Russell et al., 1983).

A combination of magnetic field and electron density profiles from the Pioneer Venus Orbiter (PVO) mission to Venus is shown in Fig. 1. This figure shows clearly how the plasma scale height reacts to the solar wind changes, as a result of a balance between plasma and magnetic field pressures. The left panel shows the ionospheric behaviour under a moderate magnetic field condition (value of around 60 nT at the top of the ionosphere). When the magnetic field is stronger (around 90 and 140 nT at the ionopause), the electron density profiles are completely different, as seen in the middle and right panels, respectively. Due to pressure balance, the topside ionosphere is compressed, resulting in a smaller scale height. Therefore, the ionopause is localized at altitudes closer to the planet. Such a plot has never been produced in the Mars case, simply due to the fact that no mission at Mars has ever performed these measurements simultaneously. Up to now, only a few indications have been detected on the electron density profiles (e.g. Fig. 2a and b on Withers et al. (2012) and Mendillo et al. (2006)), as well as some plasma compressions in regions

close to the periapsis after the arrival of a Coronal Mass Ejection (CME) and its associated magnetic field (Dubinin et al., 2008a, 2008b; Opgenoorth et al., 2013). All these examples were discussed without any direct magnetic field measurement, however with Mars Express, we attempt to overcome this difficulty by using data from the Mars Advanced Radar for Subsurface and Ionospheric Sounding (MARSIS) instrument (Picardi et al., 2004). The radar, in its Active Ionospheric Sounding (AIS) mode (Gurnett et al., 2005), has collected ionograms from which one can derive both the electron density and the magnitude of the local magnetic field (Gurnett et al., 2005, 2008; Akalin et al., 2010). Thus, for a given orbit, the magnetic field intensity at the location of the spacecraft is available, allowing us to assess the effect of the solar wind induced magnetic field on the shape of the topside ionosphere. In this context, the aim of this paper is to study the role of the induced magnetic field from the solar wind in the electron density behaviour. For this purpose, five orbits are analysed in the same location and very close in time: 3 with a clear induced magnetic field and 2 with no evidence of magnetic field.

2. Dataset

2.1. MARSIS data description

The Mars Advanced Radar for Subsurface and Ionospheric Sounding (MARSIS) is a 40 m tip-to-tip electric dipole antenna radar of low-frequencies (Picardi et al., 2004). When working in its subsurface mode, the instrument works as a geophysical radar sounding the subsurface of the planet. When working in its AIS mode, the radar sounds the ionosphere from the maximum density peak up to the spacecraft position (Gurnett et al., 2005). In this mode, the time delay of the signal is plotted against the carrier frequency in the so-called ionograms, which contain a frequency-dependent trace called “ionospheric echo”. By doing the inversion procedure of the ionospheric echo (Sánchez-Cano et al., 2012; Morgan et al., 2013), a vertical electron density profile of the ionospheric topside between the spacecraft and the maximum ionospheric ionization altitude can be obtained. The accuracy of the electron density measurement is about $\pm 2\%$, and the uncertainty on the altitude apparent range is about ± 6.8 km (Morgan et al., 2008). The spectrogram is the final representation of the MARSIS frequencies used (vertical axis) in the sounding along the time for one single orbit (horizontal axis).

The eccentricity of the Mars Express orbit is one of the main constraints for MARSIS operations because the periapsis is located about 275–350 km and the apoapsis is around 11,000 km above the surface (Chicarro et al., 2004). Since AIS is designed to analyse the lower altitude plasma, a typical MARSIS ionospheric sounding pass can only be done for altitudes less than 1200 km, which means only about 20 min either side of the periapsis (Gurnett et al., 2005), typically recording more than 300 ionograms per orbit. In the ionograms recorded closer to periapsis, it is common to find vertical lines at different frequencies called “plasma oscillation harmonics”, which are the local plasma frequency and their higher harmonics at the spacecraft altitude. These vertical lines become more intense as MARSIS moves closer to the periapsis and are due to distortions within the instrument preamplifier and produced in response to the transmission of the sounding pulses (Andrews et al., 2013 and references therein). The local plasma density has been extensively used in many studies, e.g. the detection of the ionopause (Duru et al., 2009) and is the key to derive the correct height of the profile (Sánchez-Cano et al., 2012; Morgan et al., 2013). Moreover, some ionograms contain additional and invaluable information registered as horizontal lines, which are called “electron cyclotron echoes”. These lines are located on the left side of the ionograms (low-frequencies) and are equally spaced in delay time, and can be used to compute the magnitude of the local magnetic field (Gurnett et al., 2008; Akalin et al., 2010). The derivation of the magnetic field is based on the assumption that the radar antennas generate an electric field which accelerates the electrons in a magnetic field medium. The magnitude of the magnetic field is derived from the measured value of the cyclotron frequency (Gurnett et al., 2008; Akalin et al., 2010). If there are no electrons close to the antennas, the radar will not record any presence of magnetic field, even if there is one. The main limitation of this kind of data is that MARSIS only measures the magnitude of the magnetic field at the spacecraft position and the direction of the magnetic field can only be retrieved after strong assumptions, such as those made in Akalin et al. (2010). The magnetic field measured by MARSIS is the sum of both internal (crustal) and external magnetic fields in the ionosphere.

2.2. Data processing

The goal of this study is to assess the effect of an induced magnetic field on the ionosphere. For that, five MEX orbits of the northern hemisphere of the planet and very close in time, i.e. 18.5 days of difference between first and last orbits, were chosen with similar conditions of solar zenith angle (SZA), solar longitude (Ls), heliocentric distance, solar activity and solar cycle phase. All of them correspond to the same geographical location (same latitude and longitude, see more detailed information at the Annexed tables), which is an area with no significant crustal magnetic field anomalies (Cain et al., 2003). Moreover, in 3 of the 5 orbits, MARSIS recorded a significant magnetic field in the full orbits as identified by the cyclotron echoes in the ionograms, whose origin is the solar wind since no crustal magnetic field is expected. In the other 2 orbits, MARSIS did not record any notable magnetic signal along the full trajectories. It could be the case that other orbits had similar characteristics to those selected in this study. However, we decided to use only the 5 closer ones to ensure the most similar possible conditions. Therefore, differences in the behaviour of those orbits can only be attributed to the presence of an induced magnetic field. Table 1 summarises the main characteristics of these 5 orbits, and Fig. 2 shows the orbit tracks through latitude, longitude, solar zenith angle, and spacecraft altitude. Data used in this study is framed by a rectangle in Fig. 2.

In order to obtain an ionospheric topside density profile from the selected orbits, the following criteria are applied:

(1) Only that part of the orbit where MARSIS was working in AIS mode can be used.
(2) Only data with similar latitudes and SZA in each of the 5 orbits have been analysed.
(3) Only ionograms with local plasma harmonics were used. This only occurs when the spacecraft is below the ionopause, which has been defined as the so-called flow velocity boundary (Duru et al., 2008).
(4) Only data with a clearly defined ionospheric trace has been considered in order to get the real critical plasma frequency.
(5) For these orbits where cyclotron harmonics are present (see above), the magnitude of the field was calculated from the estimation of the cyclotron frequency, as described in Akalin et al. (2010).

Fig. 3 shows the spectrograms of two orbits. The upper panel corresponds to orbit 3140 (orbit with no measured magnetic field), and the bottom panel to orbit 3184 (orbit with a measured magnetic field). In both cases, the yellow–green horizontal lines between frequencies of 0.1 and 1.5 MHz correspond to the local plasma harmonics at the spacecraft altitude (in the ionograms

Table 1
Mars Express orbits characteristics. Main parameters of each orbit.

Mars Express orbit number	3129	3140	3151	3184	3195
Date (dd/mm/yyyy)	17/06/2006	20/06/2006	23/06/2006	03/07/2006	06/07/2006
Heliocentric distance (AU)	1.67	1.67	1.67	1.67	1.67
Ls (deg)	67.5	68.8	70.2	74.2	75.5
F10.7 (sfu, at 1 AU)	73	73	72	86	85
Latitude (North °)	4.9/34.0	2.2/33.0	−0.1/33.1	6.9/31.3	4.9/33.1
Longitude (East °)	296	295	294	291	290
Spacecraft altitude (km)	306/412	307/387	309/359	314/356	316/385
Solar Zenith Angle, SZA (deg)	46/55	45/55	43/55	39/46	37/45
Number of analysed ionograms in the selected region	31	25	44	30	38
Measured magnetic field (nT) at the location of the spacecraft	0 nT, except 4 profiles with 25 nT	0 nT in 14 profiles, and 25 nT in 11	45/62	56/69	29/45 nT, except 6 profiles with 0 nT
Crustal magnetic field (nT) from Cain et al. (2003) model	1.5/10.7	1.8/9.2	2.0/9.0	0.9/2.9	0.6/3.2
Local electron density ($\times 10^9$ e^-/m^3)	0.1/1.9	0.8/3.4	0.5/3.0	0.1/1	0.1/1.8
Peak altitude (km)	112/136	107/123	110/123	116/134	109/127
Peak electron density ($\times 10^{11}$ e^-/m^3)	0.9/1.2	1.0/1.2	1.1/1.3	1.1/1.3	1.1/1.3
Topside Total Electron Content, TEC ($\times 10^{16}$ e^-/m^2)	0.4/0.7	0.4/0.6	0.4/0.6	0.4/0.6	0.4/0.6
Plasma scale height (km)	One scale height (mean) ~64	One scale height (mean) ~41	Two scale heights, in the range 30 and 40–45	Two scale heights, in the range 35 and 45	Two scale heights, in the range 30–40 and 40–50

these are vertical lines), the central bulge corresponds to the periapsis of the Mars Express orbit, the yellow–green vertical lines between frequencies of 1.5 and 3.5 MHz correspond to the ionospheric traces, and finally the data gap in both orbits correspond to the time period when MARSIS was working in the subsurface mode. Since these two orbits were acquired over the same region and separated by only 13 days, the MEX orbit trajectory over the planet was very similar for both cases. Therefore, the dissimilarities in the spectrograms respond to changes in the ionospheric behaviour and are not related to orbital/planetary variations from one orbit to the next. In the first case (upper panel, no magnetic field), MARSIS observed a more extended ionosphere, at least up to 700 km in the inbound leg (left) and up to 1200 km in the outbound leg (right), than in the second case (bottom panel, presence of magnetic field) where the limit of the ionosphere was found below 400 km for both sides. This difference in altitude is a sign of the ionosphere compression due to the presence of an induced magnetic field.

Similar differences also appear in the individual ionograms. In Fig. 4, two representative ionograms from the pericenters of the orbits in Fig. 3 are plotted. As mentioned above, the vertical lines correspond to local plasma harmonics, while the horizontal ones correspond to the electron cyclotron periods. The upper panel is an example of a typical ionogram without a magnetic field measurement, while the central panel is an example of an ionogram with a measurement of the magnetic field. After the ionogram inversion, the very final product is the vertical topside electron density profile. Two examples of electron density profiles are shown in the bottom panel of Fig. 4, selected such that the peak density are at the same altitude. For similar conditions, a more reduced density topside is found (red profile) for the magnetic field case, similar to the observed compression in the spectrograms. This is translated into a smaller scale height in the profiles where there is evidence of a magnetic field (Sánchez-Cano et al., 2015b), as will be described later. All topside electron density profiles used in this study are documented in the Annex.

Fig. 5 displays some useful parameters obtained from these 5 orbits. This figure is split into 2 panels, with the two orbits without magnetic field on the left, and the three orbits with magnetic field on the right. For both cases, subpanels from top to bottom show the electron densities measured at the spacecraft location and at the main ionospheric peak, the altitude of the main ionospheric peak, the topside total electron content (TEC) that is the electron density integrated from the peak height up to the spacecraft altitude (Sánchez-Cano et al., 2015a), the measured magnetic field by MARSIS at the spacecraft position and the spacecraft height, respectively. We note that there are few data with measured magnetic field in the left panel. We decided however, to keep them as there are only a few measurements on each orbit in comparison to the number of ionograms with null magnetic field along the same orbit, and the magnitude of this field is generally small in comparison to the orbits of the right panel, where clearly the magnetic field is very significant in every single ionogram and constant along the whole orbits. As Fig. 5 shows, the presence of a strong magnetic field does not affect the region close to the main peak, as the peak density and peak altitude are similar for both kinds of orbits. Regarding TEC, since most of it is found in the vicinity of the main peak, this parameter should not show an important change. However, for the orbits where the magnetic field is stronger, a slightly smaller and more variable TEC than in the case without magnetization is found (e.g. SZA 48–50°). A reduction of this kind in the ionization implies a more horizontal shape to the topside, which will show by definition, a reduction in the scale height. This topside density reduction is analysed in detail in this paper.

2.3. Estimation of the plasma scale height

The scale height (H) is a very useful parameter to describe the ionospheric structure, by characterising the shape of the electron density vertical profile (Belehaki et al., 2006). This parameter provides the height range over which the plasma density changes by a factor e, and is defined as:

$$\frac{1}{H} = -\frac{1}{n_e}\frac{dn_e}{dz} \tag{1}$$

In the case of hydrostatic equilibrium and a constant temperature, the scale height has a very simple expression, which depends mainly on the temperature and mean mass of the medium (Eq. (2)):

$$H = \frac{k_B T}{mg} \tag{2}$$

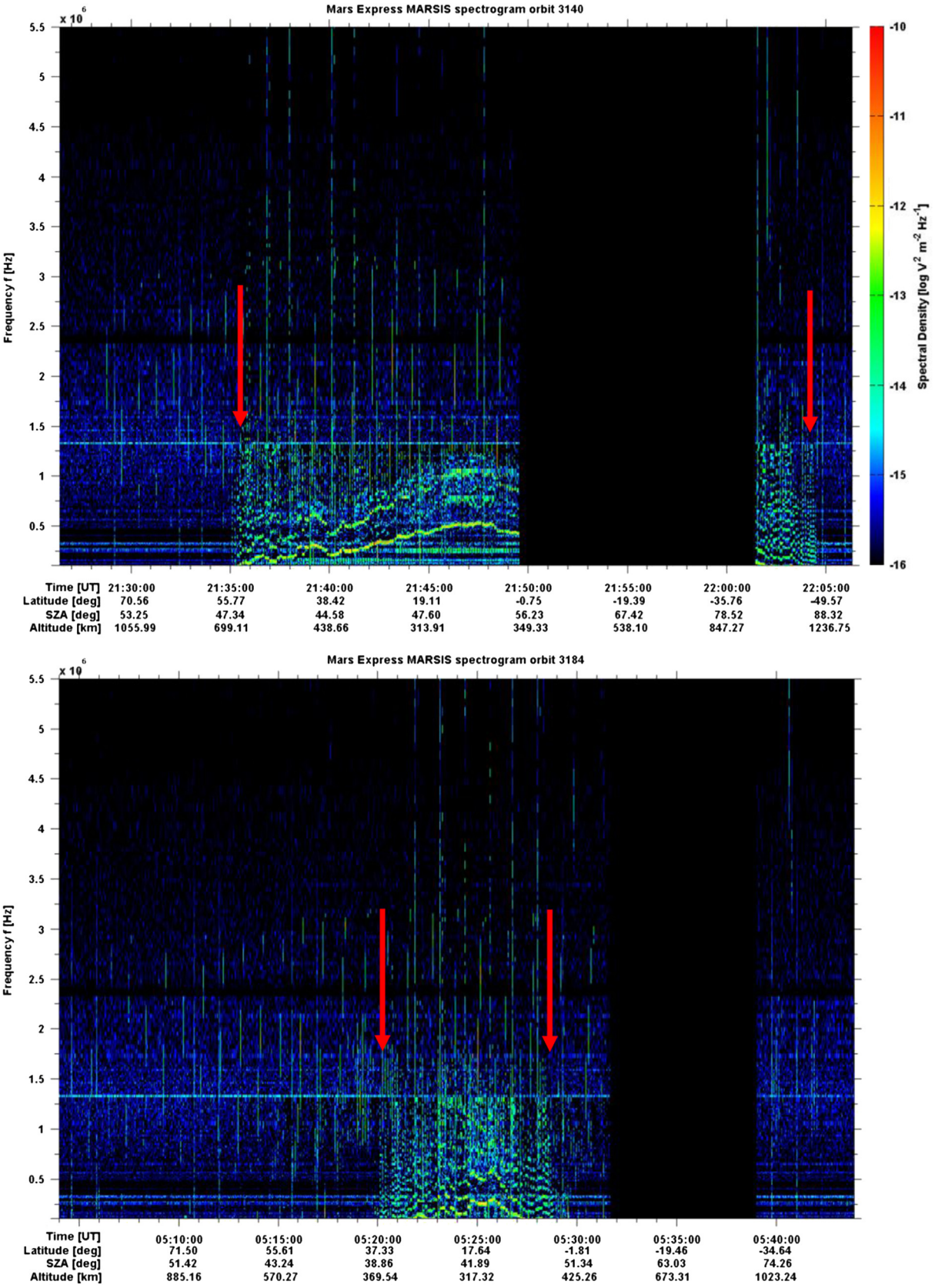

Fig. 3. MARSIS spectrograms of the two selected orbits. Upper panel: Mars Express orbit 3140 (orbit without magnetic field). Bottom panel: Mars Express orbit 3184 (orbit within magnetic field from solar wind origin). Red arrows indicate the ionosphere length. (For interpretation of the references to colour in this figure legend, the reader is referred to the web version of this article.)

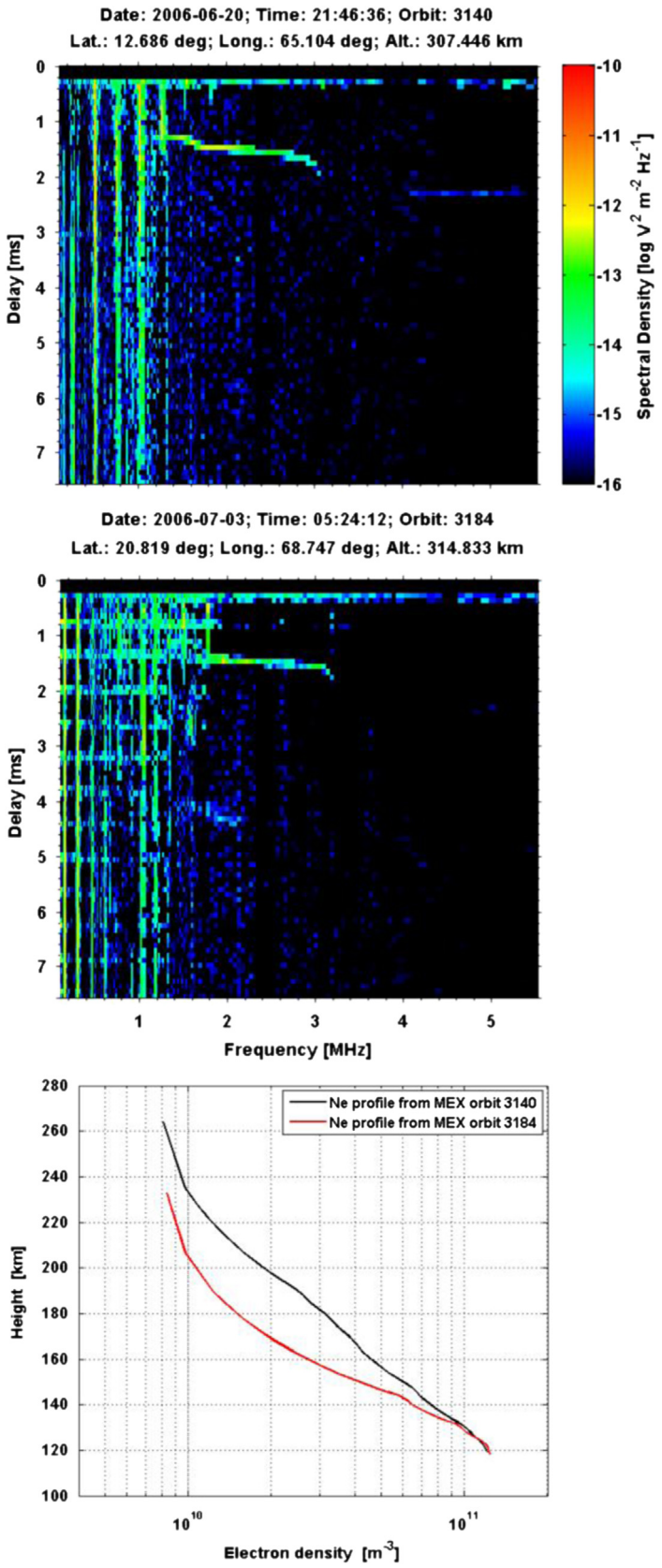

Fig. 4. Example of ionograms from the pericenter of the orbit for when there is not magnetic field at the spacecraft location (upper panel) and for when there is magnetic field (medium panel). Both ionograms belong to the orbits of Fig. 3. The horizontal echoes of the second case are caused in last instance due to the presence of a magnetic field at the spacecraft surroundings. In the bottom panel, two typical electron density profiles from these orbits.

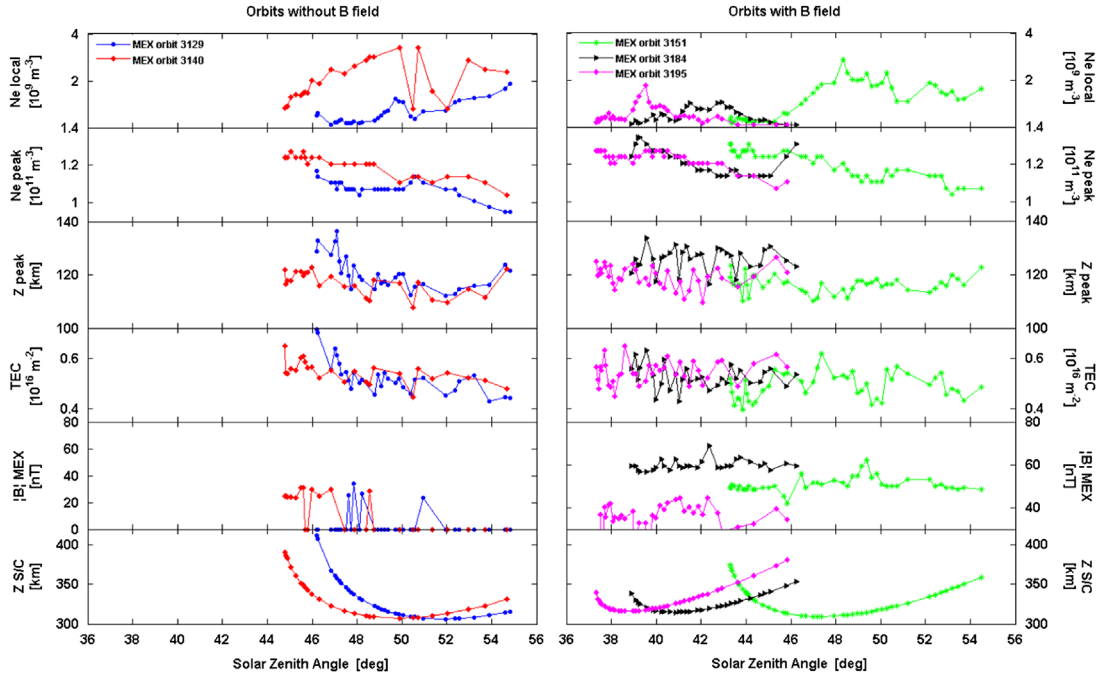

Fig. 5. Solar zenith angle series of the main characteristics of the 5 Mars Express orbits of this study. The panels of the figures show from the top to the bottom: local and peak electron densities, peak altitude, total electron content of the topside ionosphere, magnitude of the magnetic field measured by MARSIS and spacecraft altitude. Note that all the panels have the same scale at each orbit, except the MARSIS magnetic field one.

where k_B is the Boltzmann constant, T is the temperature of the medium, m is its mass and g the gravity.

The ionospheric plasma is characterized by different regimes, which have a significant impact on the scale height. We can effectively distinguish between two regimes:

- In the upper part of the ionosphere, we can assume hydrostatic equilibrium for the plasma and thus equate Eq. (1) and Eq. (2), with T being the plasma temperature and m the average mass of the ions (the major ion being O_2^+ in the main ionization region).
- In the chemical dominated region, i.e. at altitudes below ~180–200 km, the production rate varies as the neutral concentration just above the peak of production. If we consider that the speed of the reaction of recombination between ions and electrons is second order in electron concentration, then the scale height that can be derived is half the scale height obtained from Eq. (2) for the neutrals, where m corresponds to the mass of CO_2, main component of the Martian atmosphere, and T to the neutral temperature.

The latter scale height is the one used by the Chapman theory, which has been largely demonstrated to be the best formulation to describe the Martian ionosphere behaviour in the photochemically-controlled region (e.g. Gurnett et al., 2005; Pi et al., 2008; Němec et al., 2011; Sánchez-Cano et al., 2013). Note that since both scale heights have different meanings, their values are also different, the plasma scale height being always larger than the neutral. Therefore, both parameters allow retrieval of the temperature and behaviour of the neutrals and of the plasma, as well as their response to the solar wind inputs. The scale height obviously varies with altitude, reflecting different processes at work at different heights.

In this paper, the plasma scale height has been used to study the effect of the solar wind induced magnetic field in the ionosphere. This parameter has been deduced directly from the electron density profile. An example of plasma scale height is given in Fig. 6 for orbit 3151, where two scale heights were identified: 42 km just above the ionospheric peak and within the photochemically-controlled region, and 29 km, for the altitude above, in a region more dominated by transport processes. The so-called transition altitude, which is explained in the next subsection, is at the interface between those two regions.

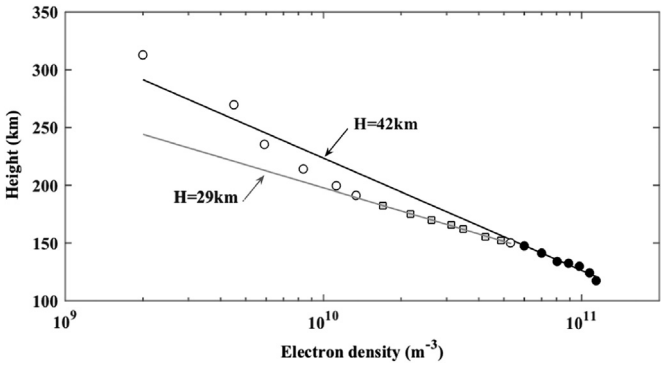

Fig. 6. Electron density profile number 169 of orbit 3151 from Mars Express. Black dots belong to the photochemical-controlled part of the ionosphere, characterised by a scale height of 42 km. White squares are the electron density points corresponding to the ionospheric region controlled by transport and magnetic field. The lower part of this region is characterised by a scale height of 29 km. A lower scale height is an indication of the compression of the ionosphere due to a penetrating induced magnetic field. White circles correspond to the rest of the profile.

2.4. Estimation of the transition altitude for the induced magnetic field

An important feature of the atmosphere-solar wind interaction is the penetration (or not) of the induced magnetic field to the plasma, and, if so, down to which altitude. Numerical simulations have shown that for an induced magnetic field of about 30–60 nT, the transition altitude is around 150 km (e.g. Shinagawa and Cravens, 1989; Witasse, 2000). This is not a sharp transition, its width being around 25 km. Our goal is to determine one typical value to compare with the predictions of numerical simulations. Although

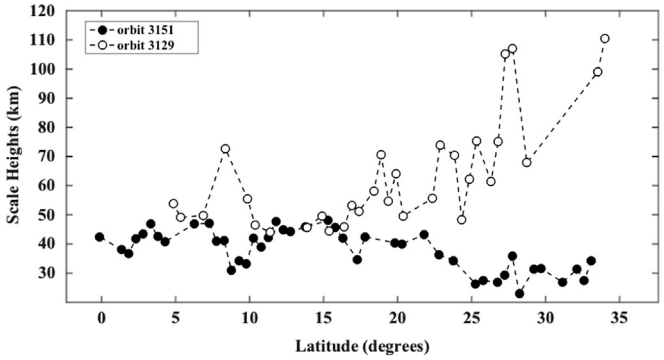

Fig. 7. Plasma scale heights of the photochemical-controlled region of the ionosphere as a function of the latitude. Mars Express orbit 3129 in white dots and Mars Express orbit 3151 in black dots.

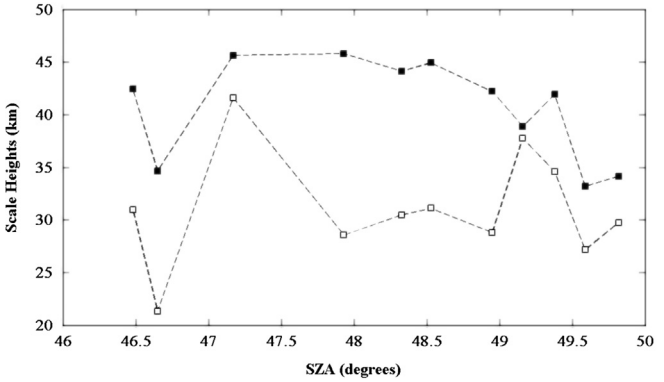

Fig. 8. Mars Express Orbit 3151: values of the two plasma scale heights found in the profiles, as a function of solar zenith angle. Black squares: plasma scale height of the photochemical-controlled region (region in the profile close to the peak). White squares: plasma scale height of the region under the influence of the magnetic field penetration (diffusive region, top part of the profile).

there is not a clear definition, we define the transition altitude as the altitude above which the ionosphere is no longer governed by pure photochemical processes. Above this height, the dynamics are strongly dependant on the penetration of an induced magnetic field. To establish this limit, we have considered the transition point where the density departs by an empirical value of 7% below the slope defined by the scale height above the peak.

3. Results

An observable variation in the electron density distribution is detected when a magnetic field is induced in the ionosphere, as Figs. 3–5 and Table 1 have already demonstrated. In order to analyse in detail the role of this magnetic field in the ionospheric structure, we select examples of orbits with and without induced magnetic field in the ionosphere, orbits 3151 and 3129 respectively. An analogous behaviour was found for the other orbits (see Annex). In particular, for orbit 3151 (magnetic field case), five different regimes can be identified in the profiles:

1. Ionograms 125–141 (latitudes 33.1–25.3 North degrees): No ionospheric compression, diffusive equilibrium at high altitudes, no clear effect of an induced magnetic field. Only a slight ionospheric compression can be seen, corresponding to ionograms 132–133.
2. Ionograms 144–152 (latitudes 23.8–19.8 North degrees): the densities follow a constant scale height.
3. Ionograms 156–173 (latitudes 17.8–9.3 North degrees): Here, the plasma is clearly compressed, with a clear transition altitude.
4. Ionograms 174–177 (latitudes 8.8–7.3 North degrees): the densities follow a constant scale height.
5. Ionograms 179–192 (latitudes 6.3 to −0.13 North degrees): Again, a compression is detected, with a smaller amplitude than for ionograms 156–173.

The ionosphere in orbit 3151 appears more compressed than in orbit 3129, where a unique scale height is always found.

The plasma scale heights have been estimated for each ionogram of both orbits, as explained in Section 2.3. Fig. 7 shows the results of the scale height from the photochemical region (i.e. close to the electron density peak) of each orbit, as a function of the latitude. The scale heights are smaller in the magnetized case, being on average between 30 and 40 km for orbit 3151 (back dots) and, between 50 and 110 km for orbit 3129 (white dots). Moreover as mentioned before, the induced magnetic field in the ionosphere produced a very compressed region in that part of orbit 3151 defined as 3 (latitude range 17.8–9.3 North degrees). The profiles belonging to this regime are characterised by two scale heights: the first immediately above the ionospheric peak in the photochemical controlled region, and the second at higher altitudes, in the diffusive region controlled by the induced magnetic field. Fig. 8 displays these two kinds of scale heights found in this orbit as a function of solar zenith angle. The photochemical region scale height is represented by black dots and the diffusive region scale height appears in white dots. This second scale height is generally 10 km smaller than the photochemical one, indicating the compressive role of the induced magnetic field at higher altitudes in the profiles.

For that latitude region, the transition altitudes (see Section 2.4) lie mainly in the altitude band 147–166 km, completely compatible with results from modelling (e.g. Shinagawa and Cravens, 1989). Tables in the Annex give the value of this transition altitude, together with other parameters derived from both kinds of orbits.

The scale height and the transition altitude are good indicators of the compression of the plasma, as explained above. Further in this analysis, the pressure balance has been analysed for orbit 3151 since it is a useful parameter to diagnose the interaction between the ionosphere and the solar wind (e.g. Zhang and Luhmann, 1992). The objective is to perform additional tests to evaluate if the magnetic field could penetrate down to the transition altitude in that orbit. Theoretically, the induced magnetic field penetrates down to an altitude where the magnetic pressure equals the plasma thermal pressure. Below, the thermal pressure is higher than the magnetic pressure, and the magnetic field intensity decreases to zero because of the magnetic diffusion effect. Since the available dataset does not give access to all necessary observables such as a magnetic field profile and temperatures, the pressure balance assumption has been used to find whether reasonable values can be estimated for these parameters.

On one hand, the plasma pressure, P_p, is given by:

$$P_p = n_e k_B T_p \tag{3}$$

where n_e is the electron density, k_B is Boltzmann's constant, and T_p the plasma temperatures. On the other hand, the magnetic pressure, P_B, is given by:

$$P_B = \frac{B^2}{2\mu_0} \tag{4}$$

where B is the intensity of the magnetic field and μ_0 the permeability of the free space. After equating Eqs. (3) and (4) and considering Eq. (1) for the plasma population of the region above the main peak, the magnetic field intensity can be estimated as follows:

$$B = \sqrt{2\mu_0 m_p g n_e H} \tag{5}$$

where in this case, m is the average ion mass, which has been assumed for the transition altitude: around 90% of O_2^+ and 10% of CO_2^+ (e.g. Shinagawa and Cravens, 1989). It is important to remark here that the estimation of both the scale height and the magnetic field is done around the transition altitude only, where both pressures are expected to be equal. The hypothesis is not valid below or above this specific altitude.

The results are illustrated in Fig. 9, where the magnetic field measured by the radar at the spacecraft location, at about 350 km (solid black circles) for orbit 3151, and the estimated magnetic field from the pressure balance, at about 170 km (white circles), versus the solar zenith angle for the same orbit are plotted. At the transition altitude, on average, the calculated magnetic field is 27 nT, while the averaged measured value by MARSIS at the higher altitude is 51 nT. The results are again, fully compatible with earlier results. To show the degree of penetration of this induced field, Fig. 10 shows the values of the magnetic field calculated for the transition altitude for orbit 3151 and for the other 2 orbits with magnetic field of this study after following the same procedure than in orbit 3151. The strongest magnetic fields, obviously, have more power of penetration and therefore for those cases, the transition altitude is found at lower levels. The balance between magnetic and thermal pressures gives therefore a good estimation of the induced magnetic field in the ionosphere at the transition altitude.

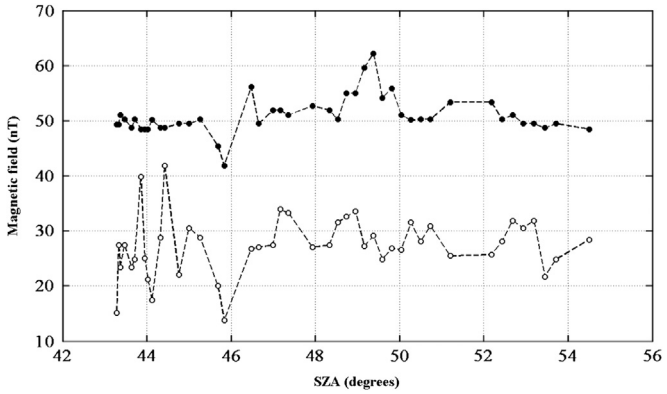

Fig. 9. Magnitude of magnetic field measured by MARSIS in orbit 3151 at the spacecraft position (black dotted-line) and magnitude of the magnetic field at the transition altitude derived from the pressure balance (white dotted-line) for the same orbit, versus solar zenith angle.

The data and the results were subsequently compared with a model of the ionosphere of Mars (Witasse, 2000; Witasse et al., 2002, 2003; Morel et al., 2004; Sánchez-Cano et al., 2015b). This one-dimensional model is based on a coupling between a kinetic and a fluid code. The kinetic part is a stationary Boltzmann approach, which describes the energetic electron flux. The electron source may be either the incoming solar wind electrons or photoelectrons due to EUV photo-ionisation. The fluid part is an eight-moment time-dependent model which solves the transport equations of the different charged species up to the heat flow. This code has been extensively and successfully used to describe the Earth's ionosphere (e.g. Lummerzheim and Lilensten, 1994; Diloy et al., 1996; Blelly et al. 2005). Its adaptation to the Martian conditions requires several important physical changes in order to take into account the interaction between the Interplanetary Magnetic Field (IMF) that drapes the planet and the upper atmosphere. The model computes, as a function of altitude, a number of ionospheric parameters, including the electron and six ion densities, vertical plasma velocities and temperatures and induced magnetic field. The neutral atmosphere is basically taken from Viking or Mariner conditions, depending on solar activity. However, some adjustments are made on the concentration profiles in order to fit the ionospheric profiles, with a given imposed horizontal magnetic field at the top of the ionosphere, in a case of a magnetized ionosphere. The magnetic field value at the top is chosen arbitrarily, typically in the range 20–100 nT, and is adjusted consistently with the atmosphere in order to get the best fit on the ionospheric profile.

For this comparison, one profile (from ionogram 169 of orbit 3151) was selected, and the results are shown in Fig. 11. Three parameters have been plotted: the electron density (top panel), the plasma temperature (middle panel) and the induced magnetic field (bottom panel). For the modelling run, the geophysical conditions (solar activity, solar zenith angle, heliocentric distance) of orbit 3151 were chosen and set as input parameters in the model. The magnetic field value at the top of the atmosphere (500 km) has been set at 57 nT, such that it can match exactly the measured value at 313 km.

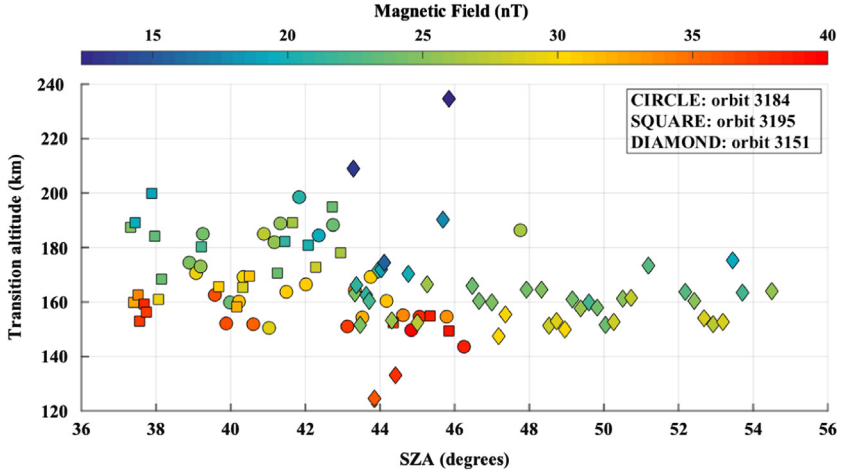

Fig. 10. Distribution of the magnetic field at the transition altitude, obtained from the balance of pressures versus solar zenith angle, for the 3 selected Mars Express orbits with magnetic field. The colour-bar stand for the magnitude of this field. (For interpretation of the references to colour in this figure legend, the reader is referred to the web version of this article.)

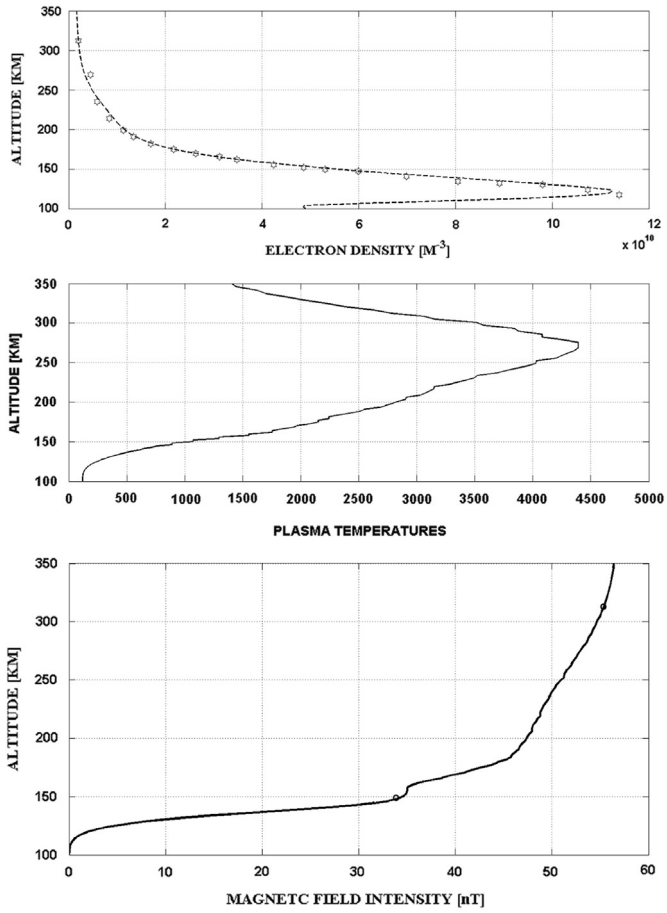

Fig. 11. Comparison with a numerical model of the ionosphere. The data correspond to the profile 169 from orbit 3151. The electron density vertical profile is displayed on the top panel, where the data are labelled with white stars, while the model is the dashed line. The comparison is excellent. The plasma temperature profile is plotted in middle panel. In this case, the model is the solid dark line, and the temperature deduced from the scale height in good agreement, around 580 K in the altitude range 115–155 km. There is a reasonable agreement between data and model. The induced magnetic field is given on the bottom panel. The model is in solid dark line, and the two circles indicate the magnetic field measured locally by the spacecraft (here at 313 km) and the magnetic field deduced from the pressure balance at the transition altitude (here at 149 km). The match is almost perfect.

The comparison between model and data is remarkable for the three panels. Regarding the electron density (top panel), the comparison between the data and the model shows an almost perfect match even in linear scale. A clear manifestation of the good behaviour of the model to reproduce both the shape of the profile as well as the electron density values, even with the presence of an induced magnetic field. One of the by-products that easily can be retrieved both from the model and the data is the temperature of the plasma population (electrons plus ions). From the data, this parameter is obtained by using the definition of scale height (Eq. (1)) and the assumptions about the ion composition as described above. Note that only the plasma scale height calculated for the closest region above the peak can be used in this equation. This plasma temperature has been compared with the temperature profile deduced from the model (medium panel). In that figure, the temperature deduced from the plasma scale height is in the range 115–150 km. There is no possibility of obtaining a temperature profile from a single scale height, only one temperature value can be retrieved in the altitude range used to obtain that scale height. There is reasonable agreement between data and model (550 K at 137 km) and the results are consistent with those presented in the Fig. 2 of Shinagawa and Cravens (1989) where a value greater than 1400 K is reached at ~160 km for electrons. Finally, in the bottom panel, the magnetic field profile obtained for the ionospheric altitude acquired from the model (solid line) is compared with the two only values obtained from the MARSIS radar: the one measured at the spacecraft position (white circle at 313 km) and the one deduced from the pressure balance (white circle at 149 km). At these altitudes the values of the magnetic field are ~55 nT and ~34 nT respectively, showing good agreement with the model and with the results from previous studies (Shinagawa and Cravens, 1989). These comparisons confirm the hypothesis that for orbit 3151, an induced and horizontal magnetic field is able to penetrate until an altitude of about 150 km, having a clear influence on the distribution of the density in the ionospheric vertical profile.

4. Conclusion

This study has shown an analysis of data acquired by the MARSIS instrument aboard Mars Express. These data, when interpreted carefully and successfully compared with modelling, indicate that an induced magnetic field can penetrate deep in the ionosphere of Mars, and strongly compresses the plasma. We list here the elements which are in favour of this conclusion:

- The ionosphere in the presence of a magnetic field is compressed compared to the ionosphere in orbits where no magnetic field is measured (see Fig. 4). In particular in orbit 3151, the vertical electron density profile exhibits a clear compression identified in 14 ionograms, which is characterised by a general smaller scale height (Fig. 6), and a change in scale height from ~40 to 45 down to ~30 km (Fig. 9). This is also confirmed with the other 2 orbits within the magnetic field regimen (Tables in Annex).
- A transition altitude is identified in orbits 3151, 3184 and 3195 at 150 km on average due to the penetration of an induced magnetic field in the ionosphere. This transition altitude is not found in orbits 3129 and 3140 where no magnetic field was recorded.
- From the pressure balance, reasonable plasma temperatures have been estimated. The value for the induced magnetic field estimated at the transition altitude matches very well the modelling results. The strongest magnetic fields have more power of penetration and the transition altitude is found at lower levels. As a consequence, the scale height is also smaller for those cases.

MAVEN should provide an updated picture of this process at work in the Mars' ionosphere. In particular, the coupling between the energetics and the magnetism can be further investigated.

Acknowledgements

MR-N and LV want to thank MetNet project (AYA2009-29967-C05-02, AYA2011-29967-C05-02). BS-C and ML acknowledge support through STFC Grants ST/K001000/1 and ST/N000749/1. The authors acknowledge the Principal Investigators of the Mars Express MARSIS instrument, the MARSIS team at the University of Iowa and the European Space Agency for making the data available on the Planetary Science Archive (http://www.rssd.esa.int/PSA). Also, MR-N wishes to thank M. Herraiz Sarachaga for useful discussions.

Annex: A

See Table 1A, Table 2A, Table 3A, Table 4A, and Table 5A.

Table 1A
Summary of the main characteristics of orbit 3129. From left to right: AIS profile number, solar zenith angle, latitude, altitude of the Mars Express spacecraft, magnetic field value deduced from MARSIS data and plasma scale height corresponding to the photochemical-controlled part of the Martian ionosphere.

Profile number	SZA (deg)	Latitude (deg)	Spacecraft altitude (km)	*B* field measured (nT)	*H* (km)
115	46.20	34.01	412.19	0	110.40
116	46.24	33.54	407.71	0	99.06
126	46.85	28.75	367.92	0	67.87
128	47.02	27.78	361.09	0	107.01
129	47.11	27.29	357.83	0	105.24
130	47.20	26.80	354.65	0	75.04
131	47.30	26.31	351.58	0	61.46
133	47.51	25.33	345.72	0	75.33
134	47.61	24.84	342.94	25.52	62.29
135	47.73	24.35	340.26	0	48.23
136	47.85	23.86	337.68	34.03	70.32
138	48.09	22.87	332.81	0	73.89
139	48.22	22.38	330.53	26.86	55.69
143	48.77	20.39	322.40	0	49.64
144	48.92	19.89	320.63	0	64.13
145	49.07	19.39	318.95	0	54.60
146	49.22	18.90	317.38	0	70.62
147	49.38	18.40	315.91	0	58.13
149	49.71	17.40	313.28	0	51.26
150	49.87	16.90	312.12	0	53.32
151	50.05	16.40	311.06	0	45.93
153	50.40	15.39	309.26	0	44.37
154	50.58	14.89	308.51	0	49.64
156	50.95	13.89	307.33	23.35	45.60
161	51.94	11.38	306.20	0	44.00
163	52.35	10.37	306.47	0	46.53
164	52.56	9.87	306.77	0	55.42
167	53.22	8.36	308.28	0	72.72
170	53.89	6.86	310.73	0	49.82
173	54.59	5.35	314.11	0	49.10
174	54.82	4.85	315.45	0	53.81

Table 2A
Same but for orbit 3140.

Profile number	SZA (deg)	Latitude (deg)	Spacecraft altitude (km)	*B* field measured (nT)	*H* (km)
120	44.79	32.96	386.79	24.99	44.98
121	44.84	32.48	382.89	24.47	33.62
122	44.89	32.00	379.07	23.82	34.54
125	45.05	30.55	368.20	23.82	34.22
128	45.26	29.09	358.18	23.35	33.46
131	45.50	27.63	349.04	31.07	42.34
132	45.59	27.14	346.18	31.07	42.86
133	45.69	26.65	343.43	0	40.62
134	45.78	26.15	340.77	0	44.58
136	45.99	25.17	335.76	29.78	36.27
139	46.33	23.69	328.99	24.47	37.84
143	46.85	21.70	321.37	29.78	41.81
147	47.42	19.70	315.38	0	37.24
150	47.89	18.20	311.97	0	42.61
153	48.40	16.70	309.49	0	42.03
154	48.57	16.20	308.87	28.58	41.33
155	48.75	15.70	308.36	0	40.82
161	49.89	12.69	307.44	0	47.26
164	50.50	11.18	308.40	0	37.23
165	50.71	10.68	308.92	0	49.90
168	51.36	9.178	311.12	0	45.13
171	52.03	7.67	314.26	0	43.11
175	52.97	5.67	319.89	0	45.33
178	53.69	4.17	325.18	0	44.05
182	54.69	2.19	333.68	0	44.74

Table 3A
Summary of the main characteristics of orbit 3151. From left to right: AIS profile number, solar zenith angle, latitude, altitude of the Mars Express spacecraft, magnetic field value deduced from MARSIS data, plasma scale height corresponding to the photochemical-controlled part of the Martian ionosphere and transition altitude.

Profile number	SZA (deg)	Latitude (deg)	Spacecraft altitude (km)	*B* field measured (nT)	*H* (km)	Transition altitude (km)
125	43.29	33.10	374.89	49.28	34.13	208.90
126	43.33	32.62	371.33	49.28	27.47	163.15
127	43.37	32.14	367.87	51.04	31.33	166.10
129	43.47	31.17	361.24	50.25	26.89	151.70
132	43.64	29.70	352.01	48.72	31.51	162.50
133	43.71	29.22	349.12	50.25	31.34	160.35
135	43.86	28.24	343.65	48.45	22.93	124.65
136	43.95	27.74	341.07	48.45	35.76	171.65
137	44.03	27.25	338.58	48.45	29.29	172.10
138	44.12	26.76	336.19	50.15	26.91	174.55
140	44.32	25.77	331.71	48.72	27.45	153.20
141	44.42	25.28	329.62	48.72	26.30	133.15
144	44.76	23.79	323.96	49.47	34.27	170.35
146	45.00	22.79	320.70	49.47	36.32	152.50
148	45.27	21.80	317.84	50.25	43.19	166.50
151	45.69	20.30	314.32	45.37	40.03	190.25
152	45.84	19.80	313.36	41.87	40.40	234.70
156	46.48	17.80	310.53	56.10	42.46	165.85
157	46.65	17.30	310.08	49.47	34.67	160.35
159	46.99	16.29	309.49	51.87	41.90	159.80
160	47.17	15.79	309.35	51.87	45.63	147.55
161	47.36	15.29	309.32	51.04	48.06	155.45
164	47.93	13.79	309.84	52.72	45.80	164.60
166	48.33	12.78	310.71	51.87	44.13	164.55
167	48.53	12.28	311.30	50.25	44.93	151.20
168	48.74	11.78	311.99	54.97	47.73	153.05
169	48.95	11.28	312.79	54.97	42.21	150.00
170	49.16	10.78	313.69	59.55	38.88	161.00
171	49.38	10.28	314.70	62.14	41.92	157.70
172	49.59	9.78	315.81	54.14	33.21	159.85
173	49.82	9.28	317.02	55.83	34.16	158.05
174	50.04	8.78	318.33	51.04	30.97	151.55
175	50.27	8.28	319.75	50.15	41.21	152.60
176	50.50	7.78	321.27	50.25	40.91	161.30
177	50.73	7.28	322.89	50.25	47.11	161.65
179	51.20	6.28	326.44	53.33	46.89	173.35
183	52.18	4.30	334.77	53.33	40.82	163.65
184	52.43	3.80	337.10	50.25	42.50	160.50
185	52.68	3.31	339.54	51.04	46.85	154.20
186	52.93	2.82	342.08	49.47	43.41	151.95
187	53.19	2.32	344.71	49.47	41.78	152.80
188	53.45	1.83	347.45	48.72	36.68	175.20
189	53.71	1.34	350.28	49.47	38.03	163.40
192	54.50	−0.13	359.37	48.45	42.48	164.05

Table 4A
Same but for orbit 3184.

Profile number	SZA (deg)	Latitude (deg)	Spacecraft altitude (km)	*B* field measured (nT)	*H* (km)	Transition altitude (km)
140	38.90	31.27	336.14	59.55	31.79	174.35
144	39.07	29.30	328.62	59.55	35.49	170.70
146	39.19	28.30	325.47	57.63	33.36	173.15
147	39.26	27.80	324.04	56.71	36.15	184.90
151	39.58	25.81	319.36	56.71	35.13	162.55
154	39.88	24.32	316.92	57.63	32.06	152.20
155	39.98	23.82	316.31	58.57	26.50	159.95
157	40.22	22.82	315.41	62.68	32.34	160.25
158	40.34	22.32	315.11	59.55	35.49	169.15
160	40.60	21.32	314.82	57.63	37.34	151.90
162	40.88	20.32	314.95	62.68	39.54	184.90
163	41.03	19.82	315.17	59.55	27.63	150.60
164	41.18	19.32	315.49	58.67	37.08	182.00
165	41.34	18.82	315.91	59.55	40.76	188.75
166	41.50	18.32	316.44	59.55	40.32	163.70
168	41.83	17.32	317.80	58.57	39.82	198.50
169	42.01	16.82	318.64	61.50	36.70	166.60
171	42.37	15.82	320.62	68.71	33.68	184.30
173	42.74	14.83	323.01	58.67	38.60	188.30
174	42.94	14.33	324.36	58.57	42.72	–
175	43.13	13.83	325.82	59.55	46.85	150.90
176	43.33	13.33	327.37	59.55	51.58	164.35
177	43.54	12.84	329.03	62.47	41.81	154.45
178	43.75	12.34	330.79	63.52	47.32	169.25
180	44.18	11.35	334.61	61.50	42.90	160.40
182	44.62	10.36	338.83	59.55	44.74	155.05
183	44.84	9.86	341.10	60.56	54.05	149.60
184	45.07	9.37	343.46	57.63	53.80	154.75
187	45.78	7.90	351.15	60.82	30.81	154.60
189	46.26	6.91	356.77	59.55	30.86	143.55

Table 5A
Same but for orbit 3195.

Profile number	SZA (deg)	Latitude (deg)	Spacecraft altitude (km)	*B* field measured (nT)	*H* (km)	Transition altitude (km)
140	37.33	33.13	337.29	–	35.90	187.45
144	37.40	31.15	329.83	–	38.50	159.85
145	37.44	30.66	328.21	–	33.37	189.15
147	37.52	29.67	325.28	36.65	43.43	162.70
148	37.56	29.17	323.97	–	42.94	152.95
150	37.68	28.18	321.65	40.46	47.36	159.40
151	37.74	27.68	320.64	35.73	43.29	156.30
153	37.89	26.68	318.94	41.55	37.96	199.80
154	37.97	26.19	318.24	42.04	34.10	184.15
155	38.06	25.69	317.64	33.71	35.76	161.05
156	38.15	25.19	317.14	35.73	33.19	168.35
158	38.35	24.19	316.46	35.03	38.45	–
159	38.46	23.69	316.28	36.35	39.61	–
160	38.58	23.19	316.19	34.86	45.35	–
163	38.95	21.69	316.56	38.30	39.31	–
164	39.08	21.20	316.89	–	38.83	–
165	39.22	20.70	317.32	33.08	34.98	180.25
167	39.51	19.70	318.49	33.08	37.26	–
168	39.67	19.20	319.23	–	36.33	165.70
169	39.83	18.70	320.08	36.34	34.75	–
170	39.99	18.20	321.02	35.17	40.34	–
171	40.16	17.70	322.07	41.02	36.90	158.15
172	40.33	17.20	323.22	39.01	38.39	165.45
173	40.51	16.71	324.48	42.39	43.19	169.65
175	40.87	15.71	327.29	43.88	37.50	–
176	41.06	15.21	328.85	44.66	40.58	–
177	41.26	14.72	330.51	38.30	36.11	170.65
178	41.45	14.22	332.28	40.34	37.19	182.30
179	41.65	13.73	334.14	37.61	43.49	189.15
180	41.86	13.23	336.11	40.83	40.48	–
181	42.07	12.74	338.18	36.99	36.29	180.75
182	42.28	12.24	340.34	44.66	37.40	172.70
184	42.72	11.26	344.98	37.61	41.97	195.00
185	42.94	10.76	347.45	29.16	37.98	178.15
188	43.63	9.29	355.45	30.80	37.02	–
191	44.35	7.82	364.33	32.48	47.27	152.45
195	45.34	5.88	377.54	39.70	53.67	154.90
197	45.85	4.91	384.72	34.36	50.95	149.35

References

Acuña, M.H., Connerney, J.E.P., Wasilewski, P., Lin, R.P., Anderson, K.A., Carlson, C.W., McFadden, J., Curtis, D.W., Mitchell, D., Reme, H., Mazelle, C., Sauvaud, J.A., d'Uston, C., Cros, A., Medale, J.L., Bauer, S.J., Cloutier, P., Mayhew, M., Winterhalter, D., Ness, N.F., 1998. Magnetic field and plasma observations at Mars: initial results of the Mars global surveyor mission. Science 279, 1676–1680.

Akalin, F., Morgan, D.D., Gurnett, D.A., Kirchner, D.L., Brain, D.A., Modolo, R., Acuña, M.H., Espley, J.R., 2010. Dayside induced magnetic field in the ionosphere of Mars. Icarus 206 (1), 104–111. http://dx.doi.org/10.1016/j.icarus.2009.03.021.

Andrews, D.J., Opgenoorth, H.J., Edberg, N.J.T., André, M., Fränz, M., Dubinin, E., Duru, F., Morgan, D., Witasse, O., 2013. Determination of local plasma densities with the MARSIS radar: asymmetries in the high-altitude Martian ionosphere. J. Geophys. Res. 118, 1–15. http://dx.doi.org/10.1002/jgra.50593.

Belehaki, A., Marinov, P., Kutiev, I., Jakowski, N., Stankov, S., 2006. Comparison of the topside ionosphere scale height determined by topside sounders model and bottomside digisonde profiles. Adv. Space Res. 37, 963–966. http://dx.doi.org/10.1016/j.asr.2005.09.014.

Blelly, P.-L., Lathuillère, C., Emery, B., Lilensten, J., Fontanari, J., Alcaydé, D., 2005. An extended TRANSCAR model including ionospheric convection: simulation of EISCAT observations using inputs from AMIE. Ann. Geophys. 23, 419–431. http://dx.doi.org/10.5194/angeo-23-419-2005.

Cain, J.C., Ferguson, B.B., Mozzoni, D., 2003. An n=90 internal potential function of the Martian crustal magnetic field. J. Geophys. Res. 108 (E2), 5008. http://dx.doi.org/10.1029/2000JE001487.

Chicarro, A., et al., 2004. The Mars Express mission: an overview. In: Wilson, Andrew (Ed.), Mars Express: the scientific payload, 2004. ESA Publications Division, Noordwijk, Netherlands, pp. 3–13.

Connerney, J.E.P., Acuña, M.H., Wasilewski, P.J., Ness, N.F., Rème., Mazelle, H.C., Vignes, D., Lin, R.P., Mitchell, D.L., Cloutier, A., 1999. Magnetic lineations in the ancient crust of Mars. Science 284, 794–798. http://dx.doi.org/10.1126/science.284.5415.794.

Cravens, T.E., 1997. Physics of Solar System Plasmas: Cambridge Atmospheric and Space Science Series. Cambridge University Press, Cambridge (ISBN 0521611946).

Diloy, P.-Y., Robineau, A., Lilensten, J., Blelly, P.-L., Fontanari, J., 1996. A numerical model of the ionosphere, including the E-region above EISCAT. Ann. Geophys. 14, 191–200. http://dx.doi.org/10.1007/s00585-996-0191-7.

Dubinin, E., et al., 2008a. Plasma environment of Mars as observed by simultaneous MEX-ASPERA-3 and MEX-MARSIS observations. J. Geophys. Res. 113, A10217. http://dx.doi.org/10.1029/2008JA013355.

Dubinin, E., et al., 2008b. Structure and dynamics of the solar wind/ionosphere interface on Mars: MEX-ASPERA-3 and MEX-MARSIS observations. Geophys. Res. Lett. 35, L11103. http://dx.doi.org/10.1029/2008GL033730.

Duru, F., Gurnett, D.A., Morgan, D.D., Modolo, R., Nagy, A.F., Najib, D., 2008. Electron densities in the upper ionosphere of Mars from the excitation of electron plasma oscillations. J. Geophys. Res. 113, A07302. http://dx.doi.org/10.1029/2008JA013073.

Duru, F., Gurnett, D.A., Frahm, R.A., Winningham, J.D., Morgan, D.D., Howes, G.G., 2009. Steep, transient density gradients in the Martian ionosphere similar to the ionopause at Venus. J. Geophys. Res. 114, A12310. http://dx.doi.org/10.1029/2009JA014711.

Edberg, N.J.T., Lester, M., Cowley, S.W.H., Eriksson, A.I., 2008. Statistical analysis of the location of the Martian magnetic pileup boundary and bow shock and the influence of crustal magnetic fields. J. Geophys. Res. 113 (A8), 1978–2012. http://dx.doi.org/10.1029/2008JA013096.

Edberg, N.J.T., Eriksson, A.I., Auster, U., Barabash, S., Bösswetter, A., Carr, C.M., Cowley, S.W.H., Cupido, E., Fränz, M., Glassmeier, K.-H., Goldstein, R., Lester, M., Lundin, R., Modolo, R., Nilsson, H., Richter, I., Samara, M., Trotignon, J.G., 2009. Simultaneous measurements of the Martian plasma boundaries by Rosetta and Mars Express. Planet. Space Sci. 57 (8–9), 1085–1096. http://dx.doi.org/10.1016/j.pss.2008.10.016.

Frahm, R.A., Winningham, J.D., Sharber, J.R., Scherrer, J.R., Jeffers, S.J., Coates, A.J., Linder, D.R., Kataria, D.O., Lundin, R., Barabash, S., Holmstrom, M., Andersson, H., Yamauchi, M., Grigoriev, A., Kallio, E., Sales, T., Riihela, P., Schmidt, W., Koskinen, H., Kozyra, J.U., Luhmann, J.G., Roelof, E.C., Williams, D.J., Livi, S., Curtis, C.C., Hsieh, K.C., Sandel, B.R., Grande, M., Carter, M., Sauvaud, J.A., Fedorov, A., Thocaven, J.J., McKenna-Lawler, S., Orsini, S., Cerulli-Irelli, R., Maggi, M., Wurz, P., Bochsler, P., Krupp, N., Woch, J., Franz, M., Asamura, K., Dierker, C., 2006. Carbon dioxide photoelectron energy peaks at Mars. Icarus 182 (2), 371–382. http://dx.doi.org/10.1016/j.icarus.2006.01.014.

Gurnett, D.A., Kirchner, D.L., Huff, R.L., Morgan, D.D., Persoon, A.M., Averkamp, T.F., Duru, F., Nielsen, E., Safaeinili, A., Plaut, J.J., Picardi, G., 2005. Radar soundings of the ionosphere of Mars. Science 310 (5756), 1929–1933. http://dx.doi.org/10.1126/science.1121868.

Gurnett, D.A., Huff, R.L., Morgan, D.D., Persoon, A.M., Averkamp, T.F., Kirchner, D.L., Duru, F., Akalin, F., Kopf, A.J., Nielsen, E., Safaeinili, A., Plaut, J.J., Picardi, G., 2008. An overview of radar soundings of the martian ionosphere from the Mars Express spacecraft. Adv. Space Res. 41, 1335–1346. http://dx.doi.org/10.1016/j.asr.2007.01.062.

Krymskii, A.M., 1992. An interpretation of the large scale ionspheric magnetic fields and the altitude distribution of the ionospheric plasma on the dayside of Venus and Mars; Venus and Mars: Atmospheres, Ionospheres and Solar Wind Interactions. Geophysical Monograph 66 AGU.

Krymskii, A.M., Breus, T., Nielsen, E., 1995. On possible observational evidence in electron density profiles of a magnetic field in the Martian ionosphere. J. Geophys. Res. 100 (A3), 3721–3730. http://dx.doi.org/10.1029/94JA03005.

Lummerzheim, D., Lilensten, J., 1994. Electron transport and energy degradation in the ionosphere: evaluation of the numerical solution, comparison with laboratory experiments and auroral observations. Ann. Geophys. 12 (10), 1039–1051. http://dx.doi.org/10.1007/s00585-994-1039-7.

Lundin, R., Barabash, S., Andersson, H., Holmström, M., Grigoriev, A., Yamauchi, M., Sauvaud, J.A., Fedorov, A., Budnik, E., Thocaven, J.J., Winningham, D., Frahm, R., Scherrer, J., Sharber, J., Asamura, K., Hayakawa, H., Coates, A., Linder, D.R., Curtis, C., Hsieh, K.C., Sandel, B.R., Grande, M., Carter, M., Reading, D.H., Koskinen, H., Kallio, E., Riihela, P., Schmidt, W., Säles, T., Kozyra, J., Krupp, N., Woch, J., Luhmann, J., McKenna-Lawler, S., Cerulli-Irelli1, R., Orsini, S., Maggi, M., Mura, A., Milillo, A., Roelof, E., Williams, D., Livi, S., Brandt, P., Wurz, P., Bochsler, P., 2004. Solar wind-induced atmospheric erosion at Mars: first Results from ASPERA-3 on Mars Express. Science 305 (5692), 1933–1936. http://dx.doi.org/10.1126/science.1101860.

Mendillo, M., Withers, P., Hinson, D., Rishbeth, H., Reinisch, B., 2006. Effects of solar flares on the ionosphere of Mars. Science 311, 1135–1138. http://dx.doi.org/10.1126/science.1122099.

Morel, L., Witasse, O., Warnant, R., Cerisier, J.-C., Blelly, P.-L., Lilensten, J., 2004. Diagnostic of the dayside ionosphere of Mars using the Total Electron Content measurement by the NEIGE/Netlander experiment: an assessment study. Planet. Space Sci. 52 (7), 603–611. http://dx.doi.org/10.1016/j.pss.2003.12.007.

Morgan, D.D., Gurnett, D.A., Kirchner, L.D., Fox, J.L., Nielsen, E., Plaut, J.J., 2008. Variation of the Martian ionospheric electron density from Mars Express radar soundings. J. Geophys. Res. 113, A09303. http://dx.doi.org/10.1029/2008JA013313.

Morgan, D.D., Witasse, O., Nielsen, E., Gurnett, D.A., Duru, F., Kirchner, D.L., 2013. The processing of electron density profiles from the Mars Express MARSIS topside sounder. Radio Sci. 48 (3), 197–207. http://dx.doi.org/10.1002/rds.20023.

Němec, F., Morgan, D.D., Gurnett, D.A., Duru, F., Truhlík, V., 2011. Dayside ionosphere of Mars: empirical model based on data from the MARSIS instrument. J. Geophys. Res 116, E07003. http://dx.doi.org/10.1029/2010JE003789.

Opgenoorth, H.J., Andrews, D.J., Franz, M., Lester, M., Edberg, N.J.T., Morgan, D., Duru, F., Witasse, O., Williams, A.O., 2013. Mars ionospheric response to solar wind variability. J. Geophys. Res. 118 (10), 6558–6587. http://dx.doi.org/10.1002/jgra.50537.

Pi, X., Edwards, C., Hajj, G., Ao, C., Romans, L., Callas, J., Mannucci, A., Asmar, S., Kahan, D., 2008. A Chapman-Layers Model for Mars. JPL Publication.

Picardi, G., Biccari, D., Seu, R., Plaut, J., Johnson, W.T.K., Jordan, R.L., Safaeinili, A., Gurnett, D.A., Huff, R., Orosei, R., Bombaci, O., Calabrese, D., Zampolini, E., 2004. Mars Express: A European mission to the red planet, MARSIS: Mars Advanced Radar for Subsurface and Ionosphere Sounding. European Space Agency Publication Division. SP-1240, Noordwijk, Netherlands. pp. 51–70.

Russell, C.T., Vaisberg, O., 1983. The interaction of the solar wind with Venus. In: Hunten, D.M., Colin, L., Donahue, T.M., Moroz, V.I. (Eds.), Venus. The University of Arizona Press, Tuscon, pp. 873–940.

Russell, C.T., 1992. The Pioneer Venus Mission, in Venus and Mars: Atmospheres, Ionospheres And Solar Wind Interactions. Geophys. Monog., 66. AGU

Sánchez-Cano, B., Witasse, O., Herraiz, M., Radicella, S.M., Bauer, J., Blelly, P.-L., Rodríguez-Caderot, G., 2012. Retrieval of ionospheric profiles from the Mars Express MARSIS experiment data and comparison with radio occultation data. Geosci. Instrum. Methods Data Syst. 1 (1), 77–84. http://dx.doi.org/10.5194/gi-1-77-2012.

Sánchez-Cano, B., Radicella, S.M., Herraiz, M., Witasse, O., Rodríguez-Caderot, G., NeMars, 2013. An empirical model of the martian dayside ionosphere based on Mars Express MARSIS data. Icarus 225 (1), 236–247. http://dx.doi.org/10.1016/j.icarus.2013.03.021.

Sánchez-Cano, B., Morgan, D.D., Witasse, O., Radicella, S.M., Herraiz, M., Orosei, R., Cartacci, M., Cicchetti, A., Noschese, R., Kofman, W., Grima, C., Mouginot, J., Gurnett, D.A., Lester, M., Blelly, P.-L., Opgenoorth, H., Quinsac, G., 2015a. Total electron content in the martian atmosphere: a critical assessment of the Mars Express MARSIS dataset. J. Geophys. Res. http://dx.doi.org/10.1002/2014JA020630

Sánchez-Cano, B., Lester, M., Witasse, O., Milan, S.E., Hall, B.E.S., Blelly, P.-L., Radicella, S.M., Morgan, D.D., 2015b. Evidence of scale height variations in the Martian ionosphere over the solar cycle. J. Geophys. Res. Space Phys., 120. http://dx.doi.org/10.1002/2015JA021949.

Shinagawa, H., Cravens, T.E., 1989. A one-dimensional multispecies magnetohydrodynamic model of the dayside ionosphere of Mars. J. Geophys. Res. 94 (A6), 6506–6516. http://dx.doi.org/10.1029/JA094iA06p06506.

Shinagawa, H., Cravens, T.E., 1992. The ionospheric effects of a weak intrinsic magnetic field at Mars. J. Geophys. Res. 97 (E1), 1027–1035. http://dx.doi.org/10.1029/91JE02720.

Shinagawa, H., 1996. A two-dimensional model of the Venus ionosphere: 1. Unmagnetized ionosphere. J. Geophys. Res. 101 (A12), 26911–26919. http://dx.doi.org/10.1029/96JA01361.

Shinagawa, H., 2004. The ionospheres of Venus and Mars. Adv. Space Res. 33, 1924–1931. http://dx.doi.org/10.1016/j.asr.2003.06.028.

Witasse, O., 2000. Modélisation des Ionosphères planétaires et de leur Rayonnement: la Terre et Mars (Ph.D. Thesis). Laboratoire de Planétologie de Grenoble, France.

Witasse, O., Dutuit, O., Lilensten, J., Thissen, R., Zabka, J., Alcaraz, C., Blelly, P.-L., Bougher, S.W., Engel, S., Andersen, L.H., Seiersen, K., 2002. Prediction of a CO_2^{2+} layer in the atmosphere of Mars. Geophys. Res. Lett. 29 (8), 12–63. http://dx.doi.org/10.1029/2002GL014781.

Witasse, O., Dutuit, O., Lilensten, J., Thissen, R., Zabka, J., Alcaraz, C., Blelly, P.-L., Bougher, S.W., Engel, S., Andersen, L.H., Seiersen, K., 2003. Correction to "Prediction of a CO_2^{2+} layer in the atmosphere of Mars". Geophys. Res. Lett. 30, 7. http://dx.doi.org/10.1029/2003GL017007.

Withers, P., Fallows, K., Girazian, Z., Matta, M., Häusler, B., Hinson, D., Tyler, L., Morgan, D.D., Pätzold, M., Peter, K., Tellmann, S., Peralta, J., Witasse, O., 2012. A clear view of the multifaceted dayside ionosphere of Mars. Geophys. Res. Lett. 39, 18. http://dx.doi.org/10.1029/2012GL053193.

Zhang, M.H.G., Luhmann, J.G., 1992. Comparisons of peak ionosphere pressures at Mars and Venus with incident solar wind dynamic pressure. J. Geophys. Res. 97 (E1), 1017–1025. http://dx.doi.org/10.1029/91JE02721.